PCCP



PAPER View Article Online



Cite this: DOI: 10.1039/d5cp03543k

resonance (VIPER) excitation

Luuk J. G. W. van Wilderen, (1) †** Carsten Neumann, †** Daniela Kern-Michler, †**

Optimization of vibrationally promoted electronic

Luuk J. G. W. van Wilderen, the factor of the Carsten Neumann, for Daniela Kern-Michler, for Maximiliane Horz, but Jan von Cosel, but Irene Burghardt but and Jens Bredenbeck to *a

Vibrationally promoted electronic resonance 2D-infrared (VIPER 2D-IR) spectroscopy is a powerful spectroscopic method using a sequence of IR and UV/VIS ultrafast laser pulses, which can for instance be used for 2D-IR spectral diffusion measurements beyond the vibrational lifetime or to induce subensemble-selective light-triggered processes. Its successful application depends e.g. on the intensities of the pulsed laser beams, their exact wavelengths, pulse timings and polarizations as well as on sampledependent parameters such as concentration and optical pathlength. In this work a systematic experimental and theoretical approach is taken to optimize different parameters of the detected signals. Notably, when going from low to high optical density in the UV/VIS range, the VIPER 2D-IR signal can transition from being proportional to being inversely proportional to the number of molecular absorbers present in the sample. A reversal in signal sign can be induced simply by tuning the UV/VIS pump wavelength. Exploring these and other experimental variables provides a detailed insight into the molecular parameters that govern the amplitude of the observed VIPER 2D-IR signal. This study aims to assist in the design of VIPER 2D-IR experiments that achieve the largest possible signal amplitudes as well as obtain optimal chemical contrast between different co-existing molecular species that can be excited and observed. It also provides important insight for other experimental techniques that are based on the modulation of the UV/VIS cross-section by IR excitation.

Received 14th September 2025, Accepted 21st October 2025

DOI: 10.1039/d5cp03543k

rsc.li/pccp

Introduction

The infrared (IR) spectral range offers detailed insight into molecular structure and often allows the distinction of even very similar species via specific bands in their IR spectra. In contrast, the UV/VIS spectra of similar species often exhibit substantial band overlap, impeding their selective excitation in mixtures. However, UV/VIS excitation is frequently required to populate electronically excited states and initiate photochemical and photophysical processes. Thus, combining the possibilities of UV/VIS excitation with the selectivity of IR excitation is of great interest for mixtures of similar molecules. Vibrationally promoted electronic resonance (VIPER) excitation solves this problem by first applying a resonant, selective IR_{pump} pulse, followed by an off-resonant UV/VIS_{pump} pulse, such that their combined sequential absorption populates the electronically excited state (Fig. 1(A) and (B)).

Using VIPER excitation, we have demonstrated selective electronic excitation and photodissociation within a mixture of isotopomers, even though their UV/VIS spectra in solution are indistinguishable. 1,2 In a conventional UV/VISpump-IRprobe experiment (i.e. TRIR, for transient IR) all isotopomers are simultaneously excited electronically, whereas a VIPERpump-IRprobe experiment with a tunable narrowband IRpump pulse (i.e. VIPER 2D-IR spectroscopy, Fig. 1(B)) monitors the electronic excitation of each isotopomer selectively. Further examples of subensemble-selective excitation by VIPER are the differentiation between hydrogen bonded and free molecules³ as well as selective excitation of solute molecules in different local solvent environments within an ionic liquid.4 In the latter cases, VIPER excitation was used to generate 2D-IR signals that did not decay with the vibrational lifetime, but rather with the much longer electronic lifetime. This enables the observation of chemical exchange processes between the corresponding subpopulations on a wide range of time scales.

In summary, VIPER excitation is particularly advantageous in the study of heterogeneous systems, where it allows to select molecules according to their IR spectrum for electronic excitation. Application examples are the generation of long-lived 2D-IR signals (VIPER 2D-IR spectroscopy) for measurements of spectral diffusion and chemical exchange^{3–5} and the

^a Institute of Biophysics, Goethe University Frankfurt, Max-von-Laue-Str. 1, 60438 Frankfurt am Main, Germany. E-mail: bredenbeck@biophysik.uni-frankfurt.de, vanwilderen@biophysik.uni-frankfurt.de

b Institute of Physical and Theoretical Chemistry, Goethe University Frankfurt, Max-von-Laue Str. 7, 60438 Frankfurt am Main, Germany

[†] These authors contributed equally.

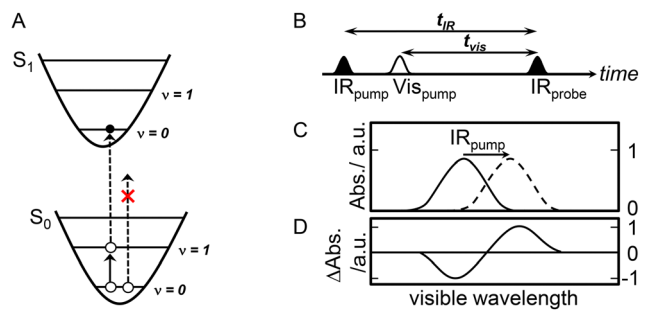


Fig. 1 Schematic representation of the VIPER 2D-IR pulse sequence and its effect on the UV/VIS absorption spectrum. Panel A shows the Jablonski diagram of the electronic ground (S_0) and excited states (S_1) as well as the levels of the vibration (ν) that are excited. Only with the aid of IR preexcitation (straight black arrow) S₁ is reached, as the energy of the UV/VIS pulse (dashed arrow) itself is non-resonant with the $S_0 \rightarrow S_1$ transition (depicted by the red cross). At non-zero temperature, low frequency modes are thermally excited (not shown), leading to a non-zero absorption cross section for photon energies below the 0-0 transition and thus a long wavelength tail in the absorption spectrum. Panel B shows the used pulse sequence. In the present work, either broadband IR or selective narrowband IR excitation is used. Alternatively, the IRpump pulse can be replaced by a pulse pair in a Fourier transform approach. Panel C schematically shows the influence of the IR_{pump} on the $S_0 \rightarrow S_1$ transition. Panel D shows the difference between the two spectra in panel C.

subensemble-selective triggering of light-induced processes, such as photochemistry.^{1,4}

Because VIPER 2D-IR spectroscopy is a fifth-order experiment, the signal sizes are relatively small when compared to third-order experiments such as conventional pump-probe or 2D spectroscopy (i.e. excited populations of 10-20% vs. 1-2% are typically achievable for third- and fifth-order experiments, respectively). A better understanding of the available parameter space that leads to successful signal detection is therefore essential. In this work, we will explore this parameter space using the laser dye coumarin 6 (C6) as it exhibits large VIPER 2D-IR signals and is easy to work with due to its stability and high solubility. Similar considerations as discussed here for VIPER 2D-IR spectroscopy apply to other experiments, where direct resonant UV/VIS excitation is replaced by combined excitation using an IR and an off-resonant UV/VIS pulse.⁶⁻⁹

Measurement principle

VIPER experiments start with the IR excitation of a specific vibrational mode, which changes the electronic absorption spectrum through vibronic couplings, 10-12 usually by shifting it to the red (Fig. 1(C) and (D)). This prepares the IR-excited molecule for subsequent excitation, shifting it into resonance with the off-resonant UV/VIS_{pump} pulse (note the dashed line in Fig. 1(A)), which promotes it to the electronically excited state.

The off-resonant UV/VIS_{pump} pulse usually is tuned to the red. On the one hand, this minimizes direct excitation of molecules without IR pre-excitation (the TRIR signal), and on the other hand it maximizes excitation of the IR pre-excited molecules (the VIPER signal). Note, that also for photon

energies lower than E(0,0) there is a non-zero probability for direct excitation, as low frequency modes are thermally excited. This leads to a residual TRIR signal as a background to the VIPER signal. Depending on the goal of the experiment it might be beneficial to either optimize the VIPER signal or the ratio of VIPER-to-TRIR signal.

In the present work, we simultaneously measure the VIPER signal, the TRIR signal and the 2D-IR signal for a given set of experimental parameters. This is possible by mechanically chopping the IR_{pump} (at a quarter of the laser's repetition rate) and VISpump pulses (at a half the repetition rate) to obtain IR_{probe} pulse intensities I for all possible combinations of IR_{pump} and VIS_{pump} $(I_{IR_{off},VIS_{off}}, I_{IR_{off},VIS_{on}}, I_{IR_{on},VIS_{off}}, I_{IR_{on},VIS_{on}})$. The TRIR and 2D-IR signals are obtained as

$$\Delta A_{\text{TRIR}} = -\log(I_{\text{IR}_{\text{off}},\text{VIS}_{\text{off}}}/I_{\text{IR}_{\text{off}},\text{VIS}_{\text{off}}}) \tag{1}$$

$$\Delta A_{2\text{DIR}} = -\log(I_{\text{IR}_{\text{opt}},\text{VIS}_{\text{off}}}/I_{\text{IR}_{\text{off}},\text{VIS}_{\text{off}}})$$
 (2)

Narrowband selective IR_{pump} pulses for VIPER and 2D-IR are generated with a Fabry-Pérot interferometer. The VIPER signal is obtained as a double difference signal

$$\Delta\Delta A_{\text{VIPER}} = -\left(\log(I_{\text{IR}_{\text{on}},\text{VIS}_{\text{on}}}/I_{\text{IR}_{\text{on}},\text{VIS}_{\text{off}}}\right) - \log(I_{\text{IR}_{\text{off}},\text{VIS}_{\text{on}}}/I_{\text{IR}_{\text{off}},\text{VIS}_{\text{off}}})$$
(3)

which is the actual VIPER signal with the residual TRIR signal resulting from direct excitation being subtracted. Alternatively, a Fourier transform (FT) implementation is possible as well.⁴

Materials and methods

Sample details

The laser dye C6 is used 'as is' and dissolved in tetrahydrofuran (THF) or perchloroethylene (PCE). All compounds are from Merck KGaA (Darmstadt, Germany). The saturated solutions are spinned down before use to remove undissolved material. The concentrations of the samples at room temperature are 20 mM in THF and 2.3 mM in PCE. The samples used for the laser measurements have a total volume of 8 ml and are continuously circulated in a transmission flow cell¹³ that has an optical pathlength of 250 µm.

Experimental setup

Steady-state UV/VIS and IR experiments are done on an UV/VIS spectrometer (U-2000; Hitachi, Japan) and an FTIR spectrometer, equipped with an MCT detector (Tensor 27; Bruker Optics GmbH & Co. KG, Ettlingen, Germany).

Time-resolved measurements are done on the laser setup that has been described earlier. 1,3 In brief, a Ti:sapphire regenerative amplifier seeded by an oscillator generates 100 fs pulses at 800 nm, 1 kHz repetition rate with 3.5 mJ per pulse (Spitfire XP and Tsunami from Spectra Physics, Newport, USA). The output fundamental is split into three beams that each pump different optical parametric amplifiers (OPAs) which generate signal and idler beams. These beams ultimately generate one probe (IR) and two pump (VIS and IR) beams. Broadband mid-IR probe light is generated by mixing signal

and idler in an AgGaS2 crystal. Narrowband mid-IR pump light (spectral width 14-18 cm⁻¹) is generated from broadband IR (about 7.5 μJ per pulse) using a Fabry-Pérot interferometer. VIS pump light from 420 nm up to almost 500 nm is generated by tripling of the signal beam (FK-800-100; EKSMA, Lithuania), from 480 nm to 520 nm by mixing the fundamental with the signal beam, and for higher wavelengths by mixing the fundamental with the idler beam. The relative polarization of all beams was parallel. The beam diameters are about 160 µm for the IR pump, 190 μ m for the Vis pump, and 90 μ m for the IR probe. Dispersed detection on a 2 \times 32 MCT array (Infrared Associates Inc., Stuart, USA) is achieved using a TRIAX 180 spectrometer with a 100 l mm⁻¹ grating (Horiba Jobin Yvon GmbH, Munich, Germany). The VIPER 2D-IR double difference absorption signals are collected using the mechanical chopper scheme described earlier.3

The general experimental conditions are the following (unless stated otherwise). The lower ring mode RM1 (see Fig. 2(B)) is pumped with narrowband IR pulses at a delay of $t_{\rm IR}$ = 2 ps for the 2D-IR measurements as this delay is longer than the pump pulse. The VISpump pulse was centered at 500 nm having a pulse energy of 0.75 μ J and a delay of t_{VIS} = 100 ps. For the VIPER 2D-IR measurements delays of $t_{\rm IR}$ = 101 ps and $t_{VIS} = 100$ ps are used.

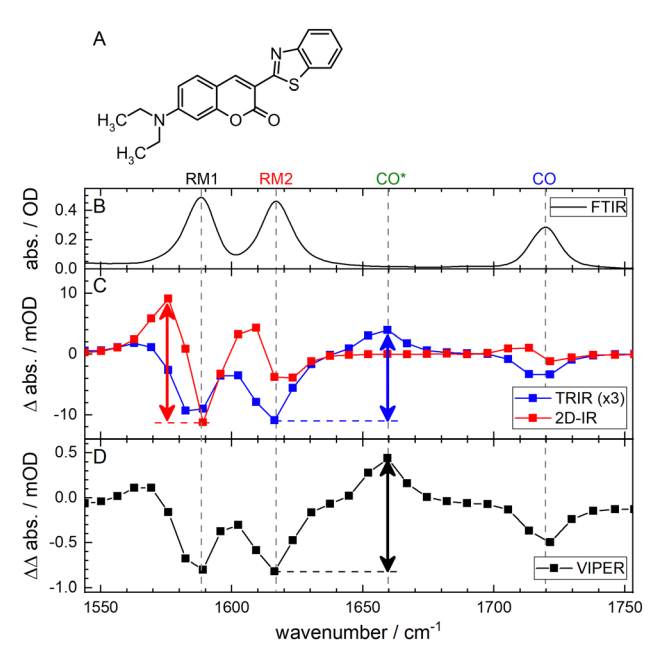


Fig. 2 Spectroscopic properties of C6 (panel A) in THF probed in the ring mode (RM) and carbonyl (CO) spectral region. The steady-state FTIR spectrum and its assignments are shown in panel B. The asterisk denotes the electronically excited state. Panels C and D depict data that are guasisimultaneously collected (using RM1 excitation with an IR_{pump} bandwidth of 14 cm⁻¹ and off-resonant VIS excitation at 517 nm). Panel C shows the 2D-IR (blue; at t_{IR} = 2 ps) and TRIR (red; at t_{VIS} = 100 ps) difference signals. The blue spectrum is scaled by a factor 3 for better visibility. Panel D shows the (double difference absorption) VIPER 2D-IR spectrum collected using $t_{\rm IR}$ = 101 ps and $t_{\rm VIS}$ = 100 ps. The black/red/blue vertical double-headed arrows define the VIPER/2D-IR/TRIR signal amplitudes that are used throughout the paper.

Computational details

The computational method is described in detail in a previous work. 10 In short, density functional theory (DFT) calculations of the respective molecular compound are done in Gaussian16 B.01¹⁴ employing the ωB97X-D functional¹⁵ in combination with the Def2-TZVP triple-zeta basis set. 16 The solvent is modelled by the polarizable continuum model (PCM). Electronically excited states are computed via time-dependent DFT (TD-DFT). Vibrationally resolved absorption spectra are obtained via analytical TD Fourier transform of the respective correlation function using the FCclasses code. 17 Subsequently, these spectra are convoluted with Gaussians and offset to match the experimentally observed spectra.

Results and discussion

The model system for the exploration of the experimental variables is the laser dye C6 (Fig. 2(A)), as it exhibits large VIPER 2D-IR signals and is easy to work with due to its stability and high solubility. Its FTIR spectrum (Fig. 2(B)) contains 3 main features in the 1550-1750 cm⁻¹ spectral region assigned to ring (RM) and carbonyl (CO) modes. Resonant VIS excitation leads to bleaches of each feature as well as a clear excited state absorption of the CO (denoted by the asterisk) in the TRIR spectrum of Fig. 2(C). The 2D-IR spectrum shows the same bleaches as well as corresponding downshifted positive features assigned to vibrationally excited states. RM1-mode excitation preceding non-resonant VIS excitation produces the VIPER spectrum of Fig. 2(D), which is similar but not identical to the TRIR spectrum (note for instance the shape of the bleach of excited RM1 as well as its corresponding positive part at lower wavenumbers). Note also that, due to the very high VIS absorption, it is still possible to generate a measurable TRIR signal at the used VIS pump wavelength of 517 nm in the red wavelength tail of the absorption band (see Fig. 3(B), blue symbols).

First, the parameters of the laser pulses are optimized to achieve the largest VIPER 2D-IR signals, subsequently followed by those related to the sample. Finally, computations predicting the influence of the IR pre-excitation on the electronic absorption spectrum are presented.

IR mode selection and timing

The first pulse in the VIPER 2D-IR sequence (see Fig. 1(B)) prepares the system by pre-excitation of a selected vibrational mode. Previously, it has been shown for C6 as well as for other aromatic compounds that RM excitation leads to VIPER 2D-IR signals that are larger than those after CO mode excitation. 10 The shape of the VIPER 2D-IR signal, however, remains the same, regardless which mode is pre-excited first. The reason for this observation is that the VIPER spectra after vibrational relaxation resemble the UV/VIS pump-IR probe spectrum (from now on referred to as transient-IR or TRIR).

With progressing time, the vibrationally excited population decays to its ground state. Before that happens, the non-resonant Paper PCCP

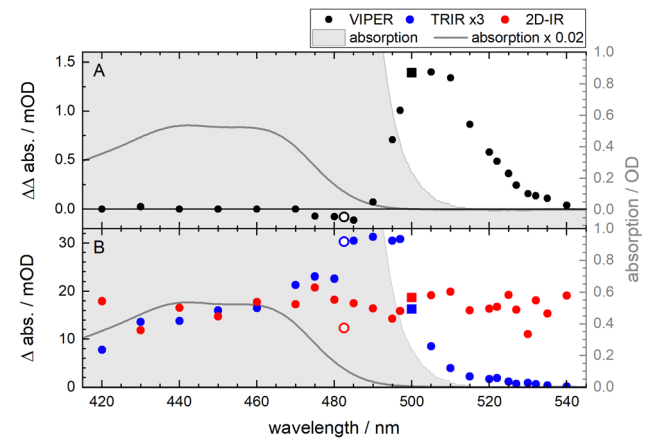


Fig. 3 UV/VIS pump wavelength dependence of the VIPER 2D-IR, TRIR and 2D-IR signal amplitudes in THF. Each symbol represents a separate measurement and its magnitude is as defined in Fig. 2. The grey area represents the (unscaled) absorption of the sample, while the grey line represents its scaled absorption ($\times 0.02$). Panel A is measured at t_{IR} = 101 ps $(IR_{pump} \text{ width: } 14-17 \text{ cm}^{-1})$ and $t_{VIS} = 100 \text{ ps}$, panel B at $t_{IR} = 2 \text{ ps}$ and $t_{VIS} = 100 \text{ ps}$ 100 ps. The blue datapoints are multiplied by a factor 3. The square symbols indicate the VIS wavelength used for the measurements shown in Fig. 6, the open symbols indicate the wavelength used for Fig. S1 (resulting in a sign-flipped VIPER 2D-IR signal).

UV/VIS_{pump} pulse can interact with the IR pre-excited population, as the IR_{nump} pulse shifts the electronic transition into resonance. Without or after decay of the pre-excitation the energy of the UV/VIS pulse is not sufficient to promote molecules to the electronically excited state and to generate a VIPER signal. It is thus important to accurately control the relative timings of the pump pulses.

The time evolution as well as the mode dependence of several VIPER 2D-IR signals is shown in Fig. 4. The narrowband IR_{pump} is tuned to one of the two shown RMs or to the CO mode. The observed time courses for all pumped modes are very similar. The maximum signals are reached within the instrument response, i.e. during the IR_{pump} pulse from the Fabry-Pérot interferometer. We therefore conclude that the largest VIPER signal is generated by the vibronic coupling of the originally excited mode. After vibrational relaxation and intramolecular vibrational relaxation (IVR) a smaller VIPER signal persists until the vibrational energy finally leaves the molecule into the solvent.3 In principle, IVR could also be exploited to use modes for selective excitation that themselves do not have a strong vibronic coupling to the electronic transition. The incorporation of a short delay between the two pump pulses would then provide the time for IVR to populate one or more vibronically coupled modes, which in consequence leads to a shift of the electronic absorption spectrum. Such a shift can in principle also occur after energy transfer from the local environment, but in the current study the described vibrational modes are all located on the same molecule.

In the IR, spectral features are often narrow and can be assigned to different species (e.g. conformations), whereas the UV/VIS bands strongly overlap. While selective UV/VIS excitation in such cases is not possible, a species can be selected via

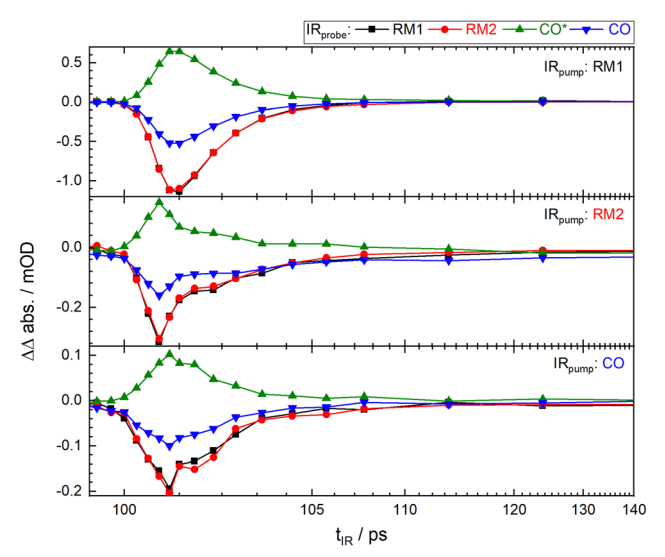


Fig. 4 Mode dependence of the VIPER 2D-IR signals in THF as function of IR delay. The narrowband IR pump (18 cm $^{-1}$ width; \sim 250 nJ per pulse) is centered at the absorption of one of the three IR modes (depicted in each panel) and the time evolution is probed at four different wavenumbers (RM1 bleach, RM2 bleach, CO* excited state absorption and CO bleach). The delay of the VIS pump pulse at 517 nm is fixed at t_{VIS} = 100 ps. A maximum population in the vibrationally excited state appears just before 101 ps.

its IR spectrum for electronic excitation in the VIPER experiment. Recently, this has opened a new avenue for photochemistry applications because it can be used for compoundspecific uncaging.1,2

UV/VIS pump wavelength

The second pump pulse is in the UV/VIS range and promotes the vibrationally excited population to the electronically excited state. As sketched in Fig. 1(C), the IR pre-excitation shifts the electronic absorption spectrum to the red, allowing the use of non-resonant UV/VIS pump wavelengths. The choice of this wavelength obviously has a large impact on the amplitude of the experimentally observed VIPER 2D-IR signals. Subtracting the shifted spectrum from that of the vibrational ground state leads to a difference spectrum that is schematically depicted in Fig. 1(D). This difference spectrum is experimentally measured here in the form of an action spectroscopy by manual scanning of the VIS wavelength (see Fig. 3(A)) and subsequent detection of the VIPER 2D-IR signal amplitude (as defined by the vertical arrow in Fig. 2(D)). This time-consuming experiment (for instance, it requires changing the wave-mixing process; see Materials and Methods) essentially reproduces the schematic induced absorption depicted in Fig. 1(D). Upon further scanning towards the blue, the maximum is followed by a signchange, before the signal is dropping below the noise level for wavelengths under 470 nm. The disappearance of the signal is in disagreement with the sketch in Fig. 1(D) and caused by the high absorption in the VIS wavelength region.

To illustrate this, the actual optical density of the sample is also plotted in Fig. 3(A) (see the grey-shaded area). The rise of **PCCP**

the VIPER 2D-IR signal initially correlates with the rise of the absorption tail towards the blue. However, the sharp increase of the VIS absorption increasingly hampers the detection of a VIPER 2D-IR signal below 470 nm (at 487 nm the OD is already about 3), as effectively all VIS pump light is already absorbed

within the first layers of the sample (see also the paragraphs on the sample's concentration and thickness below). As a consequence, a VIPER 2D-IR signal cannot be generated. The VIPER signal is caused by a modulation of the UV/VIS cross section by the IR excitation, leading to an increased or decreased population of molecules in the electronically excited state. If all UV/VIS photons are absorbed anyway, the IR_{pump} pulse cannot cause a change in the population of the electronically excited state and no VIPER signal is observed.

A benefit of the way the VIPER 2D-IR signals are measured here, i.e. via chopping and double-difference spectroscopy instead of the FT approach, is that 2D-IR and TRIR signals are collected near-simultaneously and therefore under the same conditions. Obviously, of the two single pulse experiments only the TRIR difference signal depends on the VIS pump wavelength (see the blue symbols in Fig. 3(B)). Although the signal initially scales linearly with the optical density when coming from the red, first a plateau about 15 nm wide appears, followed by a slow decrease. The reason for the deviation from the linear behaviour is currently not fully understood and cannot be solely explained by the lesser amount of pump photons (the pulse energy was kept constant, not the photon flux) towards the blue side of the spectrum. The wavelength dependency of the blue datapoints is also reproduced when tuning the OPA from the blue to the red part of the spectrum (not shown), implying that systematic measurement artifacts are unlikely. When coming from the red, it is also noted that the first appearance of the VIPER 2D-IR signal occurs at higher wavelengths than that of the TRIR signal. The reason is that the IR pre-excitation effectively allows for more off-resonant VIS excitation, providing a maximum VIPER 2D-IR signal for VIS pulses at about 497 nm.

The VIPER 2D-IR signal that is measured for pump wavelengths between 475 nm and 485 nm is negative and thus corresponds to a sign-flipped signal (see Fig. S1). In contrast, the 2D-IR and TRIR signals are not sign-flipped (not shown). Careful tuning of the VIS pump wavelength is therefore mandatory in order to optimize the VIPER 2D-IR signal's amplitude as well as its sign.

The wavelength scanning procedure used in this study entails manual optimization of the optical mixing processes to generate the same amount of pump pulse energy, rendering it a relatively time-consuming experiment. Especially if the mixing process needs to be changed altogether due to occurring degeneracies at certain wavelengths in the used non-linear optical materials, care needs to be taken that the beam sizes as well as the polarization conditions remain identical. Moreover, the light source needs to be stable in terms of output over the entire duration of the experiment. The UV/VIS wavelength dependence could in principle also be directly measured in an IR pump-UV/VIS probe¹⁸ or 2D-VE measurement, 19,20

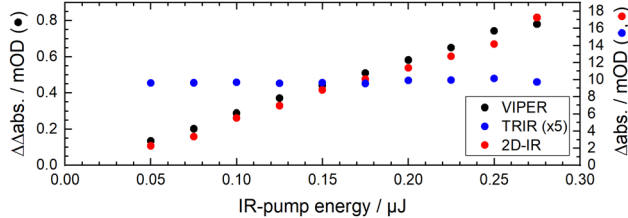


Fig. 5 IR_{pump} pulse energy dependence of the VIPER 2D-IR (black spheres), TRIR (blue) and 2D-IR (red) signal amplitudes in PCE. The approximate IR pump energy is given by the broadband IR energy/pulse divided by 20. The left-hand y-axis is for the VIPER signals, the right-hand one for IR and TRIR signals. The VIS pump wavelength is 500 nm at 0.25 μJ per pulse and at t_{VIS} = 100 ps. The signal size of the blue data points is multiplied by a factor 5 to match the scale of the red data points. The IR pump is always at $t_{IR} = 101$ ps (width 18 cm⁻¹), except for the 2D-IR experiment, where it is $t_{IR} = 2$ ps.

simplifying and accelerating the search for the optimal UV/ VIS pump wavelength and relative pump pulse timings.

IR pump energy

In order to get the highest possible VIPER-excited population, increasing the number of absorbable IR photons is crucial. In this work the narrowband IRpump pulses are generated via a Fabry-Pérot cavity, reducing the bandwidth by an estimated factor 10 and the pulse energy of the broadband IR pulses by about a factor 20. The influence of the IRpump pulse energy on the 2D-IR (red spheres) and VIPER 2D-IR (black spheres) signals are shown in Fig. 5 in PCE. Both signals scale linearly with the IR pulse energy. As expected, the size of the simultaneously measured TRIR signals does not depend on the pulse energy of the IR pump, as the VIS pump energy is invariant. The same trends are observed when applying lower and higher VIS pulse energies (see Fig. S2). The amplitude of the VIPER 2D-IR signals is therefore limited by the number of IR photons, whereas it is easily saturated by increasing the UV/VIS pulse energy (Fig. 6(A)).

Strategies to improve the IR intensity could be to reduce the diameter of the IR pump beam as well as different IR light sources, in particular using chirped-pulse difference-frequency generation to create narrowband IR pulses.

UV/VIS pump energy

After having determined the influence of the wavelength of the UV/VIS pump, its pump energy/pulse dependence is investigated. As is true for conventional pump-probe experiments such as a 2D-IR experiment, the amplitude of the VIPER 2D-IR signal is also expected to scale proportionally with the number of available UV/VIS photons. In Fig. 6 the VIS energy/pulse is gradually increased (using the optimal ${
m VIS}_{
m pump}$ wavelength for C6). Up to about 3 µJ the TRIR signal (blue spheres) scales linearly. Beyond 3 µJ the sample suffers from photodamage.

Each datapoint in Fig. 6 has a corresponding 2D-IR, TRIR and VIPER 2D-IR datapoint, as they are measured quasi simultaneously. As expected, the 2D-IR signal amplitude (red spheres) is independent of the VIS energy/pulse. The VIPER Paper

Fig. 6 VIS_{pump} pulse energy dependence of the VIPER 2D-IR (black spheres), TRIR (blue) and 2D-IR (red) signal amplitudes in THF (panel A). The left-hand *y*-axis is for the VIPER 2D-IR signals, the right-hand one for the 2D-IR and TRIR signals. The VIS pump wavelength is 500 nm (where the optical density is 0.275) at a delay of $t_{\rm VIS} = 100$ ps. The IR_{pump} is at $t_{\rm IR} = 101$ ps (width 14 cm⁻¹; ~0.275 nJ per pulse), except for the 2D-IR experiment, where $t_{\rm IR} = 2$ ps. Panel B shows the ratio of the VIPER and TRIR data (diamonds).

Vis-pump energy / µJ

2D-IR signal's pump energy dependence (black spheres) is clearly different from the other two curves. Saturation is reached around 1 μ J, *i.e.* at significantly lower pulse energies than those leading to saturation of the TRIR signal, because there are less IR-pre-excited molecules than non-pre-excited molecules (hence there are more photons/molecule).

Optimizing the experiment further for generating larger VIPER 2D-IR signals thus has to focus on increasing the IR pulse energy with which the VIPER 2D-IR signal scales linearly (Fig. 5 and Fig. S2).

Contrast for species-selective experiments

For some applications not the largest VIPER 2D-IR signal may be desired, but instead a minimum relative amount of 'background' signal caused by direct electronic excitation may be aimed for, *e.g.* if selective photochemistry of a particular species should be induced. This can be regarded as an optimization of the VIPER 2D-IR/TRIR signal ratio. In Fig. 6(B) the spectroscopic contrast is shown to be inversely proportional to the VIS_{pump} pulse energy. The IR_{pump} energy is held constant for the shown measurements. The contrast can in principle be further enhanced by using a higher IR photon flux.

An alternative approach to achieve a higher contrast could be to improve the steepness of the red flank of the electronic absorption spectrum by changing the solvent or even the molecule targeted by VIPER. For instance, the red flank of C6 in PCE is steeper than that in THF, leading to a 20-fold increase in contrast ratio (from 0.5 in Fig. 6(B) to 20 in Fig. S3).

It also needs to be stressed, however, that the presented VIPER 2D-IR data are automatically corrected for signals arising due to direct resonant UV/VIS excitation.³ Therefore, even in presence of resonant VIS absorption, species-selective experiments

are possible, as previously shown for a mixture of co-existing photocages. 1,2

Polarization dependence

In a pump–probe experiment the relative orientation of the polarizations of the pump and probe pulses determine which molecules are preferentially excited. For a molecule of the size of C6 and the used TRIR delay of $t_{\rm VIS}$ = 100 ps rotational diffusion has largely scrambled the correlation between the pulses polarization and the molecular orientation. The relative orientation of the IR_{pump} and IR_{probe} pulses was thus chosen to be parallel here. Nonetheless, it is important to mention that setting of the polarizations can lead to a maximal achievable signal gain of a factor 3 in pump–probe spectroscopy, and even a factor 15 in a three pulse experiment. Here we used parallel polarization between the two pump pulses as that resulted in the largest VIPER signal for exciting RM1 in agreement with the computed transition dipole angles (see Section 4 in the SI).

To illustrate the maximum possible range of the signal size of C6 as a function of the two relative polarization angles of the three pulses, we show the computed map in Fig. 7, which neglects rotational diffusion and thus resembles the situation for short delays $t_{\rm IR}$ and $t_{\rm VIS}$. In this plot the relative angle dependence between the VIS transition dipole and the RM1 and CO modes is shown. At first glance it is helpful to look at the ordinate, where it can be seen that the relative angle between the electronic transition dipole and the RM1 mode is about parallel (the redder the colour, the larger the signal). In fact, it is less than 20 degrees. About a factor 4 in signal size can be gained over the parallel orientation. Much less gain in signal size can be achieved for the CO mode, as the abscissa only

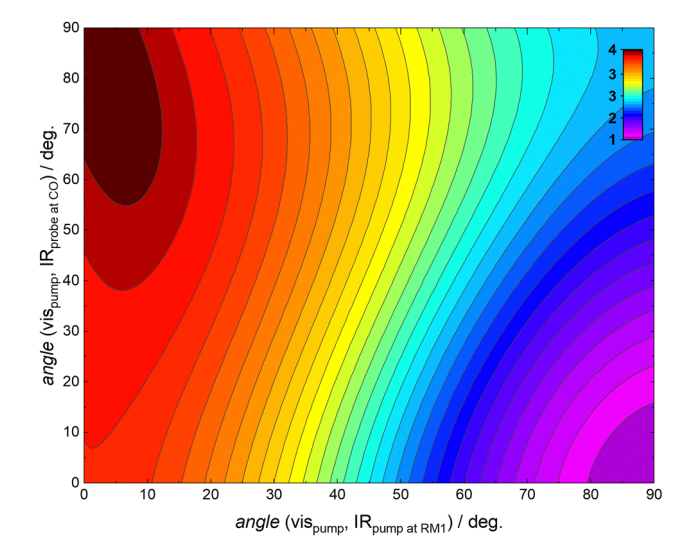


Fig. 7 Normalized computed polarization dependence for the threepulse experiment on C6 in THF after excitation of RM1. The relative angle dependence between the orientation of the IR modes (RM1 and CO) and the VIS transition dipole moment (VIS_{pump}) is shown. Higher values indicate a larger signal for a given relative polarization orientation. Fig. S4 shows the same plot for C6 in PCE.

indicates a moderate increase of about 5% (it has a relative orientation of about 65 degrees).

In general, however, careful optimization of the relative pulse timings and their polarization conditions allow a gain of more than an order in magnitude in VIPER 2D-IR signal amplitude.

Sample concentration

Besides optimizing the properties of the different laser pulses for larger VIPER 2D-IR signal amplitudes, increasing the number of molecules will generally also lead to larger signals. For the following discussion it is assumed that the electronic absorption spectrum is not modulated by intermolecular interactions. Here it is shown that, perhaps surprisingly, the VIPER 2D-IR signal amplitude can increase when lowering the concentration. This is illustrated in Fig. 8 for C6 dissolved in PCE. In analogy to Fig. 3 (where THF is the solvent) the VIS pump wavelength is again tuned in Fig. 8(A). For increasing wavelengths up to 465 nm no VIPER 2D-IR signal (black spheres) is observed. For longer wavelengths a positive signal appears. Previously, a negative signal was observed below the zero crossing of the VIPER 2D-IR signal (see Fig. 3(A)). Besides a solvent-induced shift of the electronic ground state absorption spectrum, there is however no obvious reason why the wavelength dependence of the VIPER 2D-IR signal should be fundamentally different in either solvent. In THF the (negative)

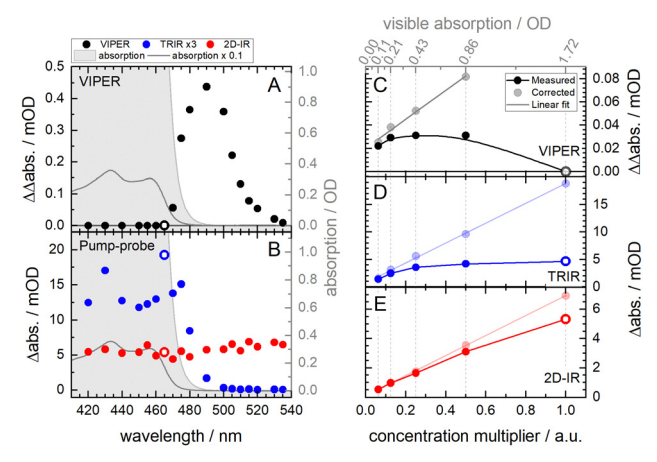


Fig. 8 VIS pump wavelength dependence and dilution series measured in PCE. Panels A and B are analogous to Fig. 3, with identical pulse timings, using $t_{IR} = 101$ ps and $t_{VIS} = 100$ ps in panel A, $t_{IR} = 2$ ps and $t_{VIS} = 101$ ps in panel B. The blue datapoints are multiplied by a factor 3. The open symbols indicate the 465 nm VIS pump wavelength at which the data in panels C-E are measured as function of subsequent sample dilution (with the starting condition also marked by the open symbol). The bold-coloured symbols are the measured data that are connected by a spline function as a guideto-the-eye, the light-coloured ones the data after correction for the sample's high optical density, the light-coloured lines are the corresponding linear fits (with slopes of about 5 mOD per OD in the IR, 2.3 mOD per OD in the VIS, and 2 mOD per sum of the OD in the IR and the VIS for the 2DIR, TRIR and VIPER data, respectively). The zero amplitude VIPER signal is not corrected. The initial sample, corresponding to a multiplier of 1, has an OD of 0.14 at RM1. The pump wavelength dependence and the dilution series are done on different samples.

VIPER 2D-IR signal actually also disappears below 470 nm, which was attributed to the high VIS absorption (see above). The same absorption effect occurs for the drop to zero amplitude in PCE. In Fig. 8(C) the VIPER 2D-IR signal amplitude at 465 nm in PCE is shown. Without dilution of the sample (corresponding to the open black symbol at a concentration multiplier factor of 1) no VIPER 2D-IR signal is detected. The absorption at this wavelength approaches OD = 2. Diluting the sample by a factor two now leads to the appearance of a (positive) VIPER 2D-IR signal. In contrast, the 2D-IR signal amplitude is approximately halved as only half the number of molecules is present. The TRIR signal also decreases, but only by a factor 1.1, meaning that saturation effects still dominate at the high present VIS optical density and used VIS pump energy, i.e. basically all VIS photons are absorbed. The deviations from linearity for the signals shown in panels C-E can be explained by the high optical density leading to reduction of the pump intensity while propagating through the sample. Linearization can be achieved by multiplying the signals by $2.303 \cdot A/(1-10^{-A})$ with A as the absorption in the respective spectral region in OD, 24-27 i.e. that at RM1 for the 2D-IR measurements, at the VIS pump wavelength for the TRIR experiments, and that of the sum of the absorptions at RM1 and the VIS pump wavelength for the VIPER data. The corrected data is shown in each panel as light-coloured spheres as well as their corresponding linear fits, showing that at high concentrations the high VIS absorption is the main factor leading to a smaller absolute size of the VIPER signal. The VIPER signal at the highest concentration (the open sphere at concentration multiplier 1) is not corrected because the measured signal size is around the noise level.

In summary, the concentration dependence of the VIPER 2D-IR signal amplitude outlined here is an additional factor to consider when apparently no or a small VIPER effect is observed. Using diluted as well as more concentrated samples can theoretically both lead to larger VIPER 2D-IR signals, depending on the overall optical density at the sum of the IR and UV/VIS absorptions.

The already mentioned IR pump-UV/VIS probe spectroscopy method (see the UV/VIS pump wavelength section above) may again provide helpful insights and provide details on the optimal VIS pump wavelength, for instance, as the position of the positive maximum may shift to the red with increasing concentration, simply caused by the growing electronic absorption.

Optical pathlength

Increasing the number of molecules the photons encounter can not only be achieved by increasing the concentration, but also by adding pathlength (while keeping the concentration constant). However, adding pathlength also adds solvent molecules, which may potentially absorb at the pump and probe wavelengths as well, thereby reducing the number of available photons that can generate the VIPER 2D-IR signal. In cases where the amount of pump or probe photons is limiting the signal size and solvent absorption is significant, thinner samples will be advantageous as they will generate larger signals.

The solvents used in this study for instance do not absorb in the VIS spectral region, but do have some absorption in the IR (PCE has one absorption feature around 1550 cm⁻¹, THF around 1460 cm⁻¹). The amplitudes of the VIPER 2D-IR signals presented in this work (see the vertical black arrow in Fig. 2(D)) are however not significantly affected by the solvent absorption in the IR. At the used pump and probe wavelengths it is therefore justified to look at the sample thickness dependence of the VIPER 2D-IR signal.

For these experiments, the optical pathlength is increased by using spacers of different thicknesses. Its influence on the signal sizes of experiments with one pump pulse (2D-IR and TRIR) and two-pump pulses (VIPER 2D-IR) in THF is shown in Fig. 9 (dark-coloured spheres). Initially all signal amplitudes scale proportionally with growing sample thickness, before showing saturation behaviour. The amplitude of the VIPER 2D-IR signal is even found to decrease beyond 250 µm (Fig. 9(A)). The optical density in the IR (the RMs have an OD of about 0.4 at 250 µm, see Fig. 2(A), so at 500 µm the OD will be about 0.8) now also leads to saturation behaviour for the 2D-IR signal. Again, and analogous to the concentration dependence discussed above (and shown in Fig. 8(C)-(E)), the high optical density is predominantly causing a decrease in observed VIPER 2D-IR signal sizes. The pathlength-dependent data can in this case also be successfully linearized (shown by the lightcoloured spheres and lines in Fig. 9). Although the saturation behaviour observed in Fig. 8 and 9 looks similar to that seen for

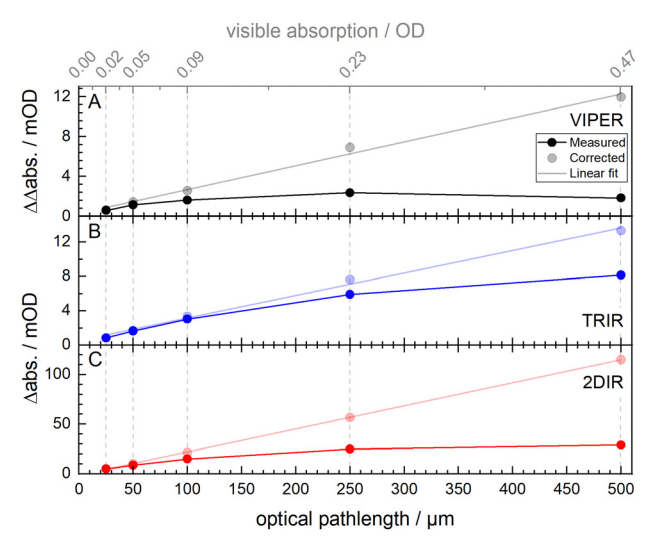


Fig. 9 Variation of optical pathlength in THF. The RM1 mode is excited with a 15 $\text{cm}^{-1}\text{-broad IR}_{\text{pump}}$ pulse (with an energy of about 0.25 μJ per pulse). The sample with an optical pathlength of 500 μm has an OD of 1.7 at RM1. The bold-coloured symbols are the measured data that are connected by a spline function as a guide-to-the-eye, the light-coloured ones the data corrected for the high optical density, the light-coloured lines their corresponding linear fits (with slopes of about 68 mOD per OD in the IR, 28 mOD per OD in the VIS, and 5.5 mOD per sum of the OD in the IR and the VIS for the 2DIR, TRIR and VIPER data, respectively). The VIS pump wavelength is 500 nm (1 μJ per pulse) and its corresponding VIS absorption is given on top of panel A. The delays in panel A are $t_{\rm IR}$ = 101 ps and t_{VIS} = 100 ps, in panel B t_{IR} = 2 ps, in panel C t_{VIS} = 100 ps.

the pump energy dependence in Fig. 6, their origin is fundamentally different (i.e. more molecules vs. more photons). In either case, both show that the amplitude of the detected signal is not simply the additive result of the individual absorptions of (IR and VIS) photons by the molecules, i.e. increasing the quantity of either will not necessarily simply lead to larger signals.

Although it is in general not always straightforward to increase the amount of UV/VIS or IR photons due to experimental limitations (e.g. by low damage thresholds of available optical materials), increasing the number of molecules via the sample thickness is a more viable and simple measure to increase the signal. It is however also shown that merely using the largest possible optical pathlength does not necessarily produce the strongest VIPER 2D-IR signals.

Simulations of the IR-induced electronic red shift

In an effort to understand the observed UV/VIS pump wavelength dependence of the VIPER 2D-IR signals depicted in Fig. 3(A), the impact of the vibrational excitation on the electronic absorption spectrum is computed as described previously.10 These results are shown in Fig. 10 and compared to the experimental data in this study. The widths of the simulated spectra are broadened by Gaussians to match the width of the experimental absorption. The electronic absorption spectrum without vibrational pre-excitation (in black) decreases in amplitude upon RM1 pre-excitation and shows a concomitant induced absorption on the red side (see Fig. 10(A)).

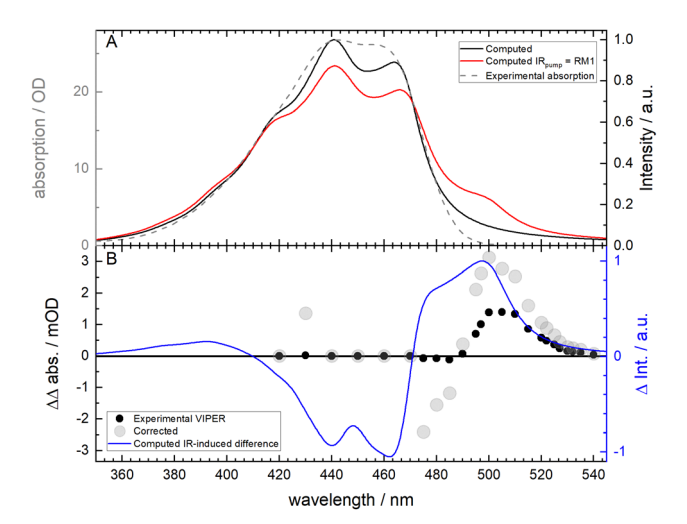


Fig. 10 Influence of the RM1 pre-excitation on the electronic absorption spectrum in THF. Panel A: comparison of the computed UV/Vis spectra with and without IR pre-excitation to the experimental absorption spectrum (same as that shown in Fig. 3). The computed spectra are shifted by \sim 40 nm and broadened with Gaussians to match the width of the experimental spectrum (grey dashed line). Panel B: comparison of the computed difference spectrum shown in A (blue spectrum) with the experimentally-derived VIPER 2D-IR wavelength dependence (black spheres, which is also shown in Fig. 3), in addition to the experimental signal that has been corrected for the high optical density (grey spheres) with an OD at RM1 of 0.49 and a VIS OD as given in panel A. The data point at 430 nm is an outlier. Fig. S5 shows the same plot for the solvent PCE.

The constructed difference spectrum qualitatively reproduces the shape of the experimental curve (see the black spheres in Fig. 10(B)). Interestingly, the wavelength at which the sign reversal is observed is about 15 nm off towards the blue, even after having wavelength-calibrated the electronic ground state absorption spectrum to the experimental spectrum. The computed difference spectrum also shows similar amplitudes of the positive and negative parts, whilst they are very different in the experimental data. As argued above, the reason for this is that the more resonant the VIS pump excitation becomes, the higher the VIS optical density is, eventually rendering it even impossible to experimentally generate a VIPER 2D-IR signal at all (see the UV/VIS pump wavelength section). Correction for the high optical density shows that the high absorption has decreased the positive part of the signal up to a factor two (compare the corrected data in light-coloured spheres to that of the black spheres). It also blue-shifts the maximum towards the simulated maximum signal (blue curve), whilst the zero-crossing is untouched. The measured positive VIPER signal remains however narrower than the simulated curve, showing only one clear positive feature as opposed to two.

Importantly, however, the presented computations provide a generic picture on the nature of the shifts in the electronic absorption spectrum. 10 Theoretical modelling reveals that the largest VIPER 2D-IR signal sizes can be expected for molecules having the largest vibronic coupling, i.e. having an electronic transition that is located in the same structural region as that of the excited vibrational mode and exhibiting large displacements along the mode upon electronic excitation. This is the reason why pre-excitation of C6's RM1 mode is leading to a strong VIPER signal (Fig. 4).

The insights these computations provide are therefore essential in understanding and optimizing VIPER signals. They will also assist in the rational design or modification of a VIPER 2D-IR chromophore that suits a particular application best, e.g. being optimal for the best VIPER/TRIR contrast, or simply generating the largest possible VIPER 2D-IR signals.

Although the computations largely agree with the experiment, some details are different (e.g. the zero-crossing point leading to the sign-reversal of the VIPER 2D-IR signal is shifted). Potential improvements that have been suggested before include the modelling of anharmonic potential energy surfaces as well the inclusion of IVR processes. 10

Conclusions

The number of potential applications for VIPER 2D-IR spectroscopy is vast, as it transfers the structure sensitivity and selectivity of IR spectroscopy to electronic excitation. The technique enables generation of long-lived 2D-IR signals that decay with the electronic instead of the vibrational lifetime, making it valuable for studies such as solvation dynamics or spectral diffusion in complex samples. Additionally, it facilitates the investigation of photophysics and photochemistry in subensembles selected by the IR pre-excitation. This work discusses several variables important for the selectivity of VIPER excitation and the contrast and size of VIPER 2D-IR signals. This is especially relevant for applications where detected signal amplitudes approach the signal-to-noise level. With VIPER 2D-IR being a fifth-order spectroscopy, small signals are a frequent obstacle to overcome. Some insights gained here on VIPER 2D-IR spectroscopy are also of interest for techniques which combine VIPER excitation with other means of detection, such as fluorescence^{8,9,28} or photocurrent.⁷

Conflicts of interest

There are no conflicts to declare.

Data availability

The data supporting this article have been included as part of the supplementary information (SI). Supplementary information: additional supporting figures and raw data to generate the figures. See DOI: https://doi.org/10.1039/d5cp03543k.

Acknowledgements

J. B. thanks the Alexander von Humboldt Foundation for the Sofia Kovalevskaja Award. The authors thank the Deutsche Forschungsgemeinschaft for funding (grant no. INST 161/722-1 FUGG, 466145756 and RTG 1986 "Complex Scenarios of Light Control").

References

- 1 D. Kern-Michler, C. Neumann, N. Mielke, L. J. G. W. van Wilderen, M. Reinfelds, J. von Cosel, F. Santoro, A. Heckel, I. Burghardt and J. Bredenbeck, J. Am. Chem. Soc., 2018, 140, 926.
- 2 L. J. G. W. van Wilderen, D. Kern-Michler, C. Neumann, M. Reinfelds, J. von Cosel, M. Horz, I. Burghardt, A. Heckel and J. Bredenbeck, Chem. Sci., 2023, 14, 2624.
- 3 L. J. G. W. van Wilderen, A. T. Messmer and J. Bredenbeck, Angew. Chem., Int. Ed., 2014, 53, 2667.
- 4 H. Brunst, H. M. A. Masood, A. R. Thun, A. Kondratiev, G. Wille, L. J. G. W. van Wilderen and J. Bredenbeck, Angew. Chem., Int. Ed., 2022, 61, e202211490.
- 5 L. J. G. W. van Wilderen and J. Bredenbeck, Angew. Chem., Int. Ed., 2015, 54, 11624.
- 6 L. Whaley-Mayda, A. Guha, S. B. Penwell and A. Tokmakoff, J. Am. Chem. Soc., 2021, 143, 3060.
- 7 N. P. Gallop, D. R. Maslennikov, N. Mondal, K. P. Goetz, Z. Dai, A. M. Schankler, W. Sung, S. Nihonyanagi, T. Tahara, M. I. Bodnarchuk, M. V. Kovalenko, Y. Vaynzof, A. M. Rappe and A. A. Bakulin, Nat. Mater., 2024, 23, 88.
- 8 C. Yan, C. Wang, J. C. Wagner, J. Ren, C. Lee, Y. Wan, S. E. Wang and W. Xiong, J. Am. Chem. Soc., 2024, 146, 1874.
- 9 H. Wang, D. Lee, Y. Cao, X. Bi, J. Du, K. Miao and L. Wei, Nat. Photonics, 2023, 17, 846.

Paper

10 J. von Cosel, J. Cerezo, D. Kern-Michler, C. Neumann, L. J. G. W. van Wilderen, J. Bredenbeck, F. Santoro and I. Burghardt, *J. Chem. Phys.*, 2017, 147, 164116.

- 11 M. Horz, H. M. A. Masood, H. Brunst, J. Cerezo, D. Picconi, H. Vormann, M. S. Niraghatam, L. J. G. W. van Wilderen, J. Bredenbeck, F. Santoro and I. Burghardt, *J. Chem. Phys.*, 2023, 158, 64201.
- 12 A. Laubereau, A. Seilmeier and W. Kaiser, *Chem. Phys. Lett.*, 1975, **36**, 232.
- 137, 30, 232.
 13 J. Bredenbeck and P. Hamm, *Rev. Sci. Instrum.*, 2003, 74, 3188.
- M. J. Frisch, G. W. Trucks, H. B. Schlegel, G. E. Scuseria, M. A. Robb, J. R. Cheeseman, G. Scalmani, V. Barone, G. A. Petersson, H. Nakatsuji, X. Li, M. Caricato, A. Marenich, J. Bloino, B. G. Janesko, R. Gomperts, B. Mennucci, H. P. Hratchian, J. V. Ortiz, A. F. Izmaylov, J. L. Sonnenberg, D. Williams-Young, F. Ding, F. Lipparini, F. Egidi, J. Goings, B. Peng, A. Petrone, T. Henderson, D. Ranasinghe, V. G. Zakrzewski, J. Gao, N. Rega, G. Zheng, W. Liang, M. Hada, M. Ehara, K. Toyota, R. Fukuda, J. Hasegawa, M. Ishida, T. Nakajima, Y. Honda, O. Kitao, H. Nakai, T. Vreven, K. Throssell, J. A. Montgomery, Jr., J. E. Peralta, F. Ogliaro, M. Bearpark, J. J. Heyd, E. Brothers, K. N. Kudin, V. N. Staroverov, T. Keith, R. Kobayashi, J. Normand, K. Raghavachari, A. Rendell, J. C. Burant, S. S. Iyengar, J. Tomasi, M. Cossi, J. M. Millam, M. Klene, C. Adamo,

- R. Cammi, J. W. Ochterski, R. L. Martin, K. Morokuma, O. Farkas, J. B. Foresman and D. J. Fox, Gaussian, Inc., Wallingford CT, 2016.
- 15 J.-D. Chai and M. Head-Gordon, *Phys. Chem. Chem. Phys.*, 2008, **10**, 6615.
- 16 F. Weigend and R. Ahlrichs, *Phys. Chem. Chem. Phys.*, 2005, 7, 3297.
- 17 J. Cerezo and F. Santoro, J. Comput. Chem., 2023, 44, 626.
- 18 R. Nakamura and N. Hamada, J. Phys. Chem. B, 2015, 119, 5957.
- 19 T. L. Courtney, Z. W. Fox, K. M. Slenkamp and M. Khalil, J. Chem. Phys., 2015, 143, 154201.
- 20 J. D. Gaynor and M. Khalil, J. Chem. Phys., 2017, 147, 94202.
- 21 U. S. Raikar, C. G. Renuka, Y. F. Nadaf, B. G. Mulimani and A. M. Karguppikar, *J. Fluoresc.*, 2006, **16**, 847.
- 22 S. S. Andrews, J. Chem. Educ., 2004, 81, 877.
- 23 J. Bredenbeck, J. Helbing and P. Hamm, J. Chem. Phys., 2004, 121, 5943.
- 24 J. F. Holland, R. E. Teets, P. M. Kelly and A. Timnick, *Anal. Chem.*, 1977, 49, 706.
- 25 C. A. Parker and W. J. Barnes, Analyst, 1957, 82, 606.
- 26 K. C. Robben and C. M. Cheatum, J. Phys. Chem. B, 2023, 127, 4694.
- 27 P. M. Donaldson, Anal. Chem., 2022, 94, 17988.
- 28 J. N. Mastron and A. Tokmakoff, J. Phys. Chem. A, 2016, 120, 9178.